



1 **Shipborne observations reveal contrasting Arctic marine, Arctic**
2 **terrestrial and Pacific marine aerosol properties**

3 Jiyeon Park¹, Manuel Dall'Osto², Kihong Park³, Yeontae Gim¹, Hyo Jin Kang^{1,4}, Eunho Jang^{1,4}, Ki-Tae
4 Park¹, Minsu Park⁵, Seong Soo Yum⁵, Jinyoung Jung¹, Bang Yong Lee¹, and Young Jun Yoon^{1,*}

5 ¹Korea Polar Research Institute, 26 Songdomirae-ro, Yeonsu-gu, Incheon 21990, South Korea

6 ²Institut de Ciències del Mar, CSIC, Pg. Marítim de la Barceloneta 37-49, 08003, Barcelona, Catalonia, Spain

7 ³Gwangju Institute of Science and Technology (GIST), 123 Cheomdangwagi-ro, Buk-gu, Gwangju 61005, Republic of
8 Korea

9 ⁴University of Science and Technology (UST), 217 Gajeong-ro, Yuseong-gu, Daejeon, Republic of Korea

10 ⁵Department of Atmospheric Sciences, Yonsei University, 50 Yonsei-ro, Seodaemun-gu, Seoul 03722, Korea

11 *Correspondence to: Y.J. Yoon (yjyoon@kopri.re.kr)

12 **Abstract**

13 There are few shipborne observations addressing the factors influencing the relationships of the
14 formation and growth of aerosol particles with cloud condensation nuclei (CCN) in remote marine
15 environments. In this study, the physical properties of aerosol particles throughout the Arctic Ocean and
16 Pacific Ocean were measured aboard the Korean ice breaker R/V Araon during the summer of 2017 for
17 25 days. A number of New Particle Formation (NPF) events and growth were frequently observed in
18 both Arctic terrestrial and Arctic marine air masses. By striking contrast, NPF events were not detected
19 in Pacific marine air masses. Three major aerosol categories are therefore discussed: (1) Arctic marine
20 (aerosol number concentration $CN_{2.5}$: $413 \pm 442 \text{ cm}^{-3}$), (2) Arctic terrestrial ($CN_{2.5}$: $1622 \pm 1450 \text{ cm}^{-3}$)
21 and (3) Pacific marine ($CN_{2.5}$: $397 \pm 185 \text{ cm}^{-3}$), following air mass back trajectory analysis. A major
22 conclusion of this study is that not only that the Arctic Ocean is a major source of secondary aerosol
23 formation relative to the Pacific Ocean; but also that open ocean sympagic and terrestrial influenced
24 coastal ecosystems both contribute to shape aerosol size distributions. We suggest that terrestrial
25 ecosystems - including river outflows and tundra - strongly affects aerosol emissions in the Arctic
26 coastal areas, possibly more than anthropogenic Arctic emissions. The increased river discharge, tundra
27 emissions and melting sea ice should be considered in future Arctic atmospheric composition and
28 climate simulations. The average CCN concentrations at a supersaturation ratios of 0.4% were 35 ± 40
29 cm^{-3} , $71 \pm 47 \text{ cm}^{-3}$, and $204 \pm 87 \text{ cm}^{-3}$ for Arctic marine, Arctic terrestrial, and Pacific marine aerosol



30 categories, respectively. Our results aim to help to evaluate how anthropogenic and natural atmospheric
31 sources and processes affect the aerosol composition and cloud properties.

32

33 **1. Introduction**

34 The climate change experienced in the Arctic is more rapid than that occurring at mid-latitudes in a
35 phenomenon known as Arctic amplification (ACIA, 2005). In the warming Arctic, the extent and
36 thickness of sea-ice have dramatically decreased over the past few decades (Stroeve et al., 2012). It has
37 been estimated that the Arctic may seasonally become sea ice-free Arctic in the next 30 years (Wang
38 and Overland, 2009). Aerosol particles in the atmosphere are a major driver of the Arctic climate (IPCC,
39 2013), as they directly affect the climate through scattering and absorbing solar radiation (Stier et al.,
40 2007), and indirectly by modifying the formation, properties, and lifetimes of clouds (Twomey, 1974).
41 These direct and indirect effects are the leading uncertainty in current climate predictions. New particle
42 formation (NPF), a predominant source of atmospheric particles, occurs through the formation of
43 nanometer-sized molecular clusters (~ 1 nm) (i.e., nucleation) and their subsequent growth into aerosol
44 particles of a few nanometers ($\sim 1 - 10$ nm) and larger (~ 10 nm) (Kulmala et al., 2004; Zhang et al.,
45 2012). NPF can significantly increase the number of aerosol particles in the atmosphere. During
46 summer, the Arctic is more isolated from anthropogenic influences (Arctic Haze) and experiences
47 comparatively pristine background aerosol conditions (Heintzenberg et al., 2015; Law and Stohl, 2007).
48 As the number concentrations of particles in the Arctic during summer are very low (of an order of $\sim 10^2$
49 cm^{-3}) (Merikanto et al., 2009), the physicochemical properties of aerosol particles in the Arctic
50 atmosphere is highly sensitive to NPF.

51 NPF events have been frequently observed within a wide range of environmental conditions at
52 various Arctic locations, such as Zeppelin (Tunved et al., 2013; Croft et al., 2016; Heintzenberg et al.,
53 2017), Tiksi (Asmi et al., 2016), Alert (Croft et al., 2016), Station Nord (Nguyen et al., 2016), and
54 Barrow (Kolesar et al., 2017), and from limited ship-based observations (Chang et al., 2011; Kim et al.,
55 2015; Heintzenberg et al., 2015). The formation and growth of particles in the Arctic atmosphere are



56 strongly influenced by marine, coastal, marginal ice, and/or anthropogenic sources. Oceanic dimethyl
57 sulfide (DMS) and other volatile organic precursors (such as isoprene, monoterpenes, and amines) play
58 important roles in the formation and growth of new particles in the Arctic (Leitch et al., 2013; Willis et
59 al., 2016; Park et al., 2017; Abbatt et al., 2019; Mungall et al., 2016). In addition, iodine oxides
60 significantly contribute to NPF in marine and coastal Arctic environments owing to emissions from
61 marine microalgae at low tide or snowpack photochemistry in ice-covered regions (Allan et al.,
62 2015; O'Dowd et al., 2002; Raso et al., 2017). Biogenic gaseous precursors released by the melting
63 Arctic sea-ice margins have also been associated with NPF (Dall'Osto et al., 2017; Willis et al., 2018).
64 Recent studies in Alaska have indicated that the formation and growth of particles are influenced by
65 emissions from oil and gas extraction activities in Prudhoe Bay (Gunsch et al., 2017; Kolesar et al.,
66 2017). Although several observations have been made in the Arctic under different environmental
67 conditions, there are few detailed size distribution analyses of particle formation and growth events
68 within the Arctic marine environment.

69 Several studies have attempted to investigate the impacts of NPF on the concentrations of cloud
70 condensation nuclei (CCN) (Willis et al., 2016; Rose et al., 2017). Model-based studies have predicted
71 that a large fraction of CCN (up to 78% of CCN at 0.2 % supersaturation) in the global atmosphere
72 results from atmospheric NPF and growth (Merikanto et al., 2009; Westervelt et al., 2014; Spracklen et
73 al., 2008). Field observations have also observed substantial increases in the concentrations of CCN due
74 to atmospheric nucleation in various environments (Pierce et al., 2012; Kalivitis et al., 2015; Kim et al.,
75 2019). Several examples of increases in the CCN concentrations after a few hours from the beginning of
76 NPF events were presented by Kim et al (2019) at King Sejong Station in Antarctic Peninsula, by Pierce
77 et al. (2012) in a forested mountain valley in western Canada, by Kalivitis et al. (2015) at an eastern
78 Mediterranean atmosphere in Grete, Greece, by Willis et al. (2016) in Arctic aircraft campaign in
79 Nunavut, Canada, and by Rose et al. (2017) at the highest atmospheric observatory on Chacaltaya,
80 Bolivia. However, due to the infrequency of aerosol measurements collected onboard ice breakers, very
81 few studies have measured the simultaneous aerosol size distribution and CCN concentrations over the



82 Arctic Ocean.

83 In this study, the physical characteristics of aerosol particles over the Arctic and Pacific Oceans were
84 investigated between August 26 and September 24, 2017, using aerosol particle monitoring instruments
85 installed on the Korean ice breaker R/V Araon. Data of the aerosol size distribution, the concentrations
86 of the total aerosol number (CN), black carbon (BC), and CCN were continuously collected using
87 various aerosol instruments. The main aims of this study were to (1) investigate the frequency and
88 characteristics of NPF and particle growth over the Arctic and Pacific Oceans, (2) determine the major
89 sources that are associated with NPF based on backward air mass trajectory analysis, and (3) explore the
90 potential contribution of NPF to the CCN concentrations in the remote marine environment.

91

92 **2. Experimental methods**

93 **2.1. Study area and ship tracks**

94 Ambient atmospheric aerosol measurements were collected over the Arctic and Pacific Oceans
95 onboard the ice breaker R/V Araon, operated by the Korea Polar Research Institute (KOPRI), Korea.
96 The ship's track is presented in Fig. 1. The cruises covered two main areas: the Arctic Ocean (including
97 both Beaufort and Chukchi Seas) and the remote Northwest Pacific Ocean. The ship departed from
98 Barrow, USA, on August 28, 2017, crossed the Beaufort (August 29-September 13, 2017) and Chukchi
99 Seas (September 15, 2017), and reached Nome, USA, on September 16, 2017. The Beaufort Sea
100 extends across the northern coasts of Alaska and the Northwest Territories of Canada. After completing
101 the Arctic survey, the ship departed from Nome, USA, on September 18, 2017, crossed the Bering Sea,
102 Sea of Okhotsk, and East Sea, and reached Busan, Korea, on September 28, 2017.

103

104 **2.2. Atmospheric aerosol measurements**

105 The aerosol sampling inlet was placed on the front deck of the ship (13 m above sea level), ahead of
106 the ship's engines to avoid any influences from the emissions of the ship's exhaust. In addition, kitchen
107 ventilation systems were connected by a plastic cylindrical pipe (~15 m length) and moved back on the



108 deck (far away from the sampling inlet) to minimize the potential effects of cooking emissions on the
109 atmospheric measurements during the sampling periods. Aerosols were sampled through a stainless
110 steel tube (inner diameter of 1/4 in, and length of ~1 m), which was connected to the various
111 instruments by electrically conductive tubing to minimize particle losses in the sampling line.

112 The physical properties of the aerosols were measured with various aerosol instruments, including
113 two condensation particle counters (TSI 3776 CPC and TSI 3772 CPC), two scanning mobility particle
114 sizers (SMPS), an optical particle sizer (OPS), an aethalometer, and a cloud condensation nuclei counter
115 (CCNC). The TSI 3776 CPC and TSI 3772 CPC measured the total number concentrations of particles
116 larger than 2.5 and 10 nm every 1 sec, respectively. The aerosol sample flow rates of TSI 3776 CPC and
117 TSI 3772 CPC were 1.5 and 1.0 lpm, respectively. The number size distributions of the particles were
118 measured using the nano SMPS every 3 min (Differential mobility analyzer (DMA): TSI 3085, CPC:
119 TSI 3776), covering a size range of 3 to 80 nm, and the standard SMPS (DMA: TSI 3081, CPC: TSI
120 3772) every 3 min, covering a size range of 10 to 300 nm. The aerosol and sheath flow rates of the
121 nano-SMPS were 1.5 and 15 lpm, respectively; and those of the standard SMPS were 1.0 and 10 lpm,
122 respectively. An OPS (TSI 3330) was used to determine the size distribution of particles in a range of
123 100 nm to 10 μm with a sample flow rate of 1.0 lpm. The BC concentration was measured using an
124 aethalometer (AE22, Magee Scientific Co., USA) to assess the influence of anthropogenic sources (such
125 as local pollution and ship emissions). The instrument uses the absorption of light at a wavelength of
126 880 nm by the ambient aerosols collected on a quartz filter tape to determine the BC concentration. The
127 flow rate through a sharp-cut 2.5 μm cyclone (BGI, Inc., USA) was set to 5 lpm and the integration time
128 was 5 min. The Droplet Measurement Technologies CCN counter (DMT CCN-100) was operated to
129 measure the CCN number concentrations. The total flow rate in the CCN counter was 0.5 lpm, and the
130 counter was operated at five different supersaturation ratios (SS) (0.2, 0.4, 0.6, 0.8, and 1.0 %) every 30
131 min. The sample and sheath flow rates of the CCN counter were 0.05 and 0.45 lpm, respectively.

132

133 **2.3. Identification of ship exhaust**



134 To obtain a data set that reflects background aerosol loading, measurement data affected by the
135 exhaust emissions of the ship's engine should be excluded prior to further data analysis. For this,
136 aerosol data were filtered based on the BC concentration, wind direction, wind speed, and total particle
137 number concentration. The data with the following properties were discarded: (1) BC concentrations
138 exceeding 100 ng m^{-3} , (2) relative wind direction against the ship's heading between 110° and 260° , as
139 this originates directly from the ship's exhaust, (3) relative wind speed lower than 2 m sec^{-1} as air
140 masses under a calm environment could become contaminated due to local turbulence, and (4) the total
141 particle number concentrations were particularly high (spike) and varied dramatically in a short time.
142 Ship plumes were clearly observed in the data collected during the campaign. Typically, the ship
143 exhaust differs from the NPF events as the enhanced number concentration during the NPF events
144 lasted for at least an hour with a low BC concentration (Ehn et al., 2010).

145

146 **2.4. Backward air mass trajectory and satellite observations**

147 The backward air mass trajectories were analyzed using version 4 of the Hybrid Single-Particle
148 Lagrangian Integrated Trajectory (HYSPPLIT) model (<http://ready.arl.noaa.gov/>) to examine their
149 relationships with the physical characteristics of aerosol particles. The 2-day air mass back trajectories
150 (48 h) were determined at hourly intervals from the ship's position at an arrival height of 50 m to
151 estimate the transport history of the air masses arriving at the observation site (Park et al., 2018). The
152 potential origins of the aerosols were divided into three categories based on the retention time of the 2-
153 day back trajectories over the three major domains: Arctic Ocean (including the Beaufort and Chukchi
154 Seas, and sea-ice region), Pacific Ocean (including the Bering Sea and Sea of Okhotsk) and land
155 (including Alaska and the eastern part of Siberia) (Fig. 1). The phytoplankton biomass was obtained by
156 calculating the chlorophyll-*a* concentration from the level-3 product of Aqua Moderate Resolution
157 Imaging Spectroradiometer at a 4 km resolution (Fig. S1). Geographical information over the ocean,
158 land and sea-ice was obtained from the sea-ice index, which was provided by the National snow and Ice
159 Data Center (NSIDC) (Fig. S2). Note that the sea-ice extent was defined as the area having an ice



160 concentration of $\geq 15\%$ (Pang et al., 2018). Air masses that intensively passed over the Beaufort and
161 Chukchi Seas and sea-ice region were categorized as Arctic Ocean originated air masses (i.e., $> 50\%$
162 retention over the ocean $> 65^\circ\text{N}$ and sea-ice region). Air masses that intensively passed over Northern
163 Alaska and the eastern Siberia were potentially affected by the Arctic tundra and categorized as land
164 originated air masses (i.e., $> 50\%$ retention over the land domain). Finally, air masses that traveled
165 through the Bering Sea and Sea of Okhotsk were categorized as air masses originated from Pacific
166 Ocean domain (i.e., $> 50\%$ retention over the ocean domain $< 65^\circ\text{N}$).

167

168 **2.5. Oceanic measurements**

169 To examine the influence of oceanic conditions on NPF and growth, seawater samples were collected
170 from sea surface at a depth of ~ 1 m by Niskin bottles. The sampling locations and methods have been
171 described previously in more detailed (Park et al., 2019). In brief, concentrations of dissolved organic
172 carbon (DOC) were measured with a Shimadzu TOC-V high-temperature combustion total organic
173 carbon analyzer. To identify the source and composition of DOC in surface seawater, three-dimensional
174 excitation-emission matrixes (EEMs) were scanned using a fluorescence spectrometer (Varian, USA).
175 The excitation wavelength range was between 250 and 500 nm, and emission between 280 and 600 nm.
176 In this study, the four major fluorescent components were classified into 4 groups; terrestrial humic
177 substances peak (A) (EX: 260 nm, EM: 380–460 nm), the terrestrial fulvic substances peak (C) (EX:
178 350 nm, EM: 420–480 nm), the marine fulvic substances peak (M) (EX: 312 nm, EM: 380–420 nm),
179 and the proteinaceous peak (T) (EX: 275 nm, EM: 340 nm) (Coble, 2007).

180

181 **3. Results and discussion**

182 **3.1. Overall particle number concentrations**

183 Fig. 2a presents a time series of the 1 hour average total particle number concentration (CN)
184 measured using TSI 3776 CPC and TSI 3772 CPC throughout the sampling periods. The number
185 concentration of particles larger than 2.5 nm ($\text{CN}_{2.5}$) or 10 nm (CN_{10}) in the Arctic and Pacific marine



186 environments had a range of approximately three orders of magnitude ($\sim 10^1 - 10^3 \text{ cm}^{-3}$). In most cases,
187 the $\text{CN}_{2.5}$ and CN_{10} concentrations were less than $\sim 2000 \text{ cm}^{-3}$, with averages of 505 ± 280 and $492 \pm$
188 264 cm^{-3} , respectively, which were in agreement with those reported in previous studies conducted at
189 other Arctic stations (Asmi et al., 2016; Burkart et al., 2017; Freud et al., 2017) and remote marine
190 regions (O'Dowd et al., 2014; Sellegri et al., 2006; Kim et al., 2019; Jang et al., 2019; Yum et al.,
191 1998; Hudson and Yum, 2002). For example, four years of observational data from the Arctic Climate
192 Observatory in Tiksi, Russia, showed that the monthly median CN concentration ranged from $\sim 184 \text{ cm}^{-3}$
193 in November to $\sim 724 \text{ cm}^{-3}$ in July (Asmi et al., 2016). Furthermore, Sellegri et al. (2006) reported CN
194 concentrations under clean marine sector conditions at Mace Head of a few hundreds of cm^{-3} (e.g., ~ 200
195 cm^{-3} in January and $\sim 450 \text{ cm}^{-3}$ in June). Elevated $\text{CN}_{2.5}$ and CN_{10} concentrations were concentrated over
196 the period from September 13 to 20, when the ship sailed over Chukchi and Bering Seas. During this
197 period, $\text{CN}_{2.5}$ and CN_{10} concentrations exceeding $\sim 2000 \text{ cm}^{-3}$ were frequently observed. The peak
198 concentrations of aerosol particles were notable, as the $\text{CN}_{2.5}$ and CN_{10} concentrations exceeded ~ 6016
199 and $\sim 5750 \text{ cm}^{-3}$, respectively.

200 To elucidate further details of the variations in $\text{CN}_{2.5}$ and CN_{10} , the particle size distributions
201 measured with the nano SMPS, standard SMPS, and OPS were divided into four size groups: nucleation
202 ($3 - 20 \text{ nm}$), Aitken ($20 - 100 \text{ nm}$), accumulation ($100 - 300 \text{ nm}$), and coarse ($> 300 \text{ nm}$ from OPS), as
203 shown in Fig. 2b–e. The average number concentrations of the nucleation-mode (N_{NUC}), Aitken-mode
204 (N_{AIT}), accumulation-mode (N_{ACC}), and coarse-mode (N_{OPS}) particles were 169 ± 142 , 201 ± 131 , $40 \pm$
205 17 , and $4 \pm 2 \text{ cm}^{-3}$, respectively. The temporal variations in N_{NUC} and N_{AIT} exhibited a distinct pattern,
206 compared to that of N_{ACC} and N_{OPS} . Overall, N_{NUC} and N_{AIT} concentrations larger than $\sim 1000 \text{ cm}^{-3}$ were
207 observed from September 13 to 20 (e.g. the ship sailed over Chukchi and Bering Seas), whereas
208 relatively high concentrations of N_{ACC} and N_{OPS} were observed from September 21 to 23 (e.g., the ship
209 sailed over Sea of Okhotsk). As shown in Fig. 2b, sudden bursts of nucleation-mode particles occurred
210 frequently, as indicated by a sudden increase in the N_{NUC} concentration rising from tens to several
211 thousands of cm^{-3} . Whenever the $\text{CN}_{2.5}$ concentration exceeded $\sim 2000 \text{ cm}^{-3}$, the N_{NUC} concentration



212 exceeded $\sim 600 \text{ cm}^{-3}$ (except for the results observed in the evening of September 18). In addition, the
213 $\text{CN}_{2.5}$ concentration was strongly correlated with the N_{NUC} concentration ($r^2 = 0.69$) (Fig. S3),
214 suggesting that the high CN concentration was mainly derived from nucleation-mode particles.
215 Instances of elevated N_{NUC} occurred along the northern coast of Alaska (September 13 – 14, 2017),
216 throughout the Chukchi Sea (September 15, 2017), near the Nome and Eastern Siberia (September 16 –
217 18, 2017), and throughout the Bering Sea (September 19 – 20, 2017). During the cruises, the satellite-
218 derived chlorophyll-*a* concentration data indicated strong biological activity over the Chukchi and
219 Bering Seas, as shown in Fig. S1. Thus, the high occurrence of nucleation-mode particles may be
220 related to multiple processes that influence the formation of secondary aerosols (e.g., oceanic biological
221 activities, regional anthropogenic emissions on land (Alaska or eastern Siberia), and terrestrial sources
222 in the tundra ecosystems of Alaska).

223

224 3.2. Case studies

225 As mentioned in Section 3.1, significant increases in N_{NUC} were frequently observed during the
226 cruise (Fig. 2 b). Typically, N_{NUC} is used to indicate the presence of newly formed particles produced by
227 gas-to-particle conversion (i.e., secondary aerosol formation) (Asmi et al., 2016; Burkart et al., 2017).
228 Here, an NPF event was defined as a sharp increase in the N_{NUC} with elevated $\text{CN}_{2.5}$ that lasted for at
229 least one hour. Fig. 3 presents contour plots of the size distributions measured using nano SMPS and
230 standard SMPS. This strong NPF and growth event occurred over the Chukchi and Bering Seas, which
231 border the western and northern sides of Alaska, suggesting that there may be a substantial source of
232 precursors in this region. Bursts of the smallest particles at the lowest detectable sizes ($\sim 2.5 \text{ nm}$) were
233 not observed, however, we hypothesize that, during the NPF event, particle formation occurred
234 elsewhere and that subsequent horizontal extension caused the particles to reach the sampling site.
235 Previously, NPF events have been identified on the regional scale in several locations around the world
236 (Kerminen et al., 2018; Németh and Salma, 2014; Vana et al., 2004; Väänänen et al., 2013). For instances,
237 Németh and Salma (2014) found that a nucleating air mass in regional NPF events may originate



238 horizontally as far as several hundreds of kilometers (~400 or 700 km) away from the sampling site. In
239 this section, case studies are discussed, including (i) marine Arctic NPF event, (ii) terrestrial Arctic NPF
240 event, and (iii) pacific marine aerosol categories. During these temporal periods, the influences of the
241 origins and pathways of air masses on the characteristics of particle formation and growth were
242 investigated.

243

244 **3.2.1. Open ocean marine Arctic NPF event case study**

245 The marine Arctic NPF event was observed on September 3, 2017, and time series plots of the
246 particle size distribution and air mass origins are presented in Fig. 4. N_{NUC} increased from 77 cm^{-3} to
247 757 cm^{-3} , while N_{AIT} varied little. The elevated number concentration of nucleation-mode particles
248 lasted for over five hours and then disappeared. Geometric mean diameter (GMD) varied from 14.6 to
249 18.2 nm with an average of 16.3 nm, indicating that particle growth hardly occurred. During the day, air
250 masses traveled over the Arctic Ocean (explicitly, 47.6, 0 and 0.4 h over the Arctic Ocean, Pacific
251 Ocean and land domain, respectively), and have been categorized as Arctic Ocean originated air masses.
252 As shown in Fig. S1, the satellite-derived chlorophyll-*a* concentration indicated a relatively high level
253 of biological activity in the ocean during the time period focused upon in this study. It was noteworthy
254 that the monthly mean chlorophyll concentration in the Beaufort and Chukchi Seas ($2.24 \pm 3.44 \text{ mg m}^{-3}$;
255 65°N – 74°N and 170°E – 120°W) was approximately 3-fold greater than that estimated in the Pacific
256 Ocean including the Bering Sea and the Sea of Okhotsk ($0.83 \pm 1.30 \text{ mg m}^{-3}$; 40°N – 65°N and
257 145°E – 168°W) (Fig. S1). Moreover, the marginal ice zone is commonly associated with intense algae
258 blooms during the melting season, therefore, significant emissions of biogenic trace gases such as DMS
259 have been detected in the sea-ice edge (Levasseur, 2013; Oziel et al., 2017). Accordingly, as our
260 measurements were collected over the Arctic Ocean onboard the ice breaker, marine biogenic sources
261 could be considered as an important factor inducing NPF events.

262 Fig. 4d shows Solar Zenith Angle (SZA) data that can be used as a proxy for solar energy reaching
263 the ground surface. We found that the NPF event occurred when the sun was below the horizon (i.e.,



264 Arctic nighttime nucleation). Typically, nucleation trends to take place preferably with high solar
265 irradiation during the daytime (Kulmala et al., 2004). In several locations, however, also nighttime
266 nucleation has been observed at Tumbarumba in Australian (Suni et al., 2008), at Värriö measurement
267 station in Finnish Lapland (Vehkamäki et al., 2004), and at a subarctic site in northern Sweden (~14 km
268 east of Abisko) (Svenningsson et al., 2008). The possible explanation for nighttime events is that the
269 actual formation and growth occurred even during daylight, but very slow growth in the Arctic and
270 marine atmosphere allowed to detect the particles (~ 8 nm) only after sunset (Vehkamäki et al., 2004).
271 Suni et al. (2008) reported that 32% of strong nighttime nucleation events (2.5 times as frequent as
272 daytime nucleation event) were appeared in the presence of a very efficient ion source such as the
273 strong radon efflux from the Tumbarumba soil. Due to their rarity, the major mechanisms for nocturnal
274 aerosol production are still unclear and require more study.

275

276 **3.2.2. Open ocean terrestrial Arctic NPF event case study**

277 The terrestrial Arctic NPF event was observed during September 13–14 2017. As shown in Fig. 5,
278 significant strong NPF events occurred frequently during this period. The number concentration of total
279 particles increased considerably, as a $CN_{2.5}$ value exceeding $\sim 6016 \text{ cm}^{-3}$ was observed during this event.
280 In addition, the average concentrations of N_{NUC} and N_{AIT} during the terrestrial Arctic NPF were $931 \pm$
281 222 and $1127 \pm 380 \text{ cm}^{-3}$, respectively. This indicates that high $CN_{2.5}$ concentration mainly contributed
282 by nucleation and Aitken-mode particles (45 and 54% of the size distribution for nucleation-mode and
283 Aitken-mode particles, respectively). GMD increased from 13.9 to 33.3 nm, indicating that the
284 nucleation-mode particles subsequently increased in size. The formation and growth of aerosol particles
285 were observed during the daytime (Fig. 5d), suggesting that photochemistry is involved. During this
286 period, air masses heavily influenced by northern Alaska. The average retention times of the 2-day back
287 trajectories arriving at the ship position over the northern Alaska, Arctic Ocean and Pacific Ocean were
288 40.8, 7.2 and 0 h, respectively (Fig. 5e). It can be seen that the photochemical reactions of precursor
289 gases (e.g., volatile organic compounds (VOCs) such as isoprene, monoterpenes, and sesquiterpenes)



290 emitted by terrestrial ecosystems in Alaska were associated with new particle formation and growth
291 (Schollert et al., 2014;TAPE et al., 2006;Kolesar et al., 2017;Ström et al., 2003).

292

293 **3.2.3. Pacific marine aerosol case study**

294 A typical aerosol scenario for Pacific marine air masses was observed on September 21–22, 2017,
295 when the air masses passed over mainly the Pacific Ocean (including the Bering Sea and Sea of
296 Okhotsk) (explicitly, 0, 47.9 and 0.1 h over the Arctic Ocean, Pacific Ocean and land domain,
297 respectively) (Fig. 1a). As shown in Fig. 6, the aerosol number concentrations exhibited a bimodal size
298 distribution, peaking at size ranges of 30 – 80 nm (Aitken mode) and 100 – 300 nm (accumulation
299 mode), respectively. In contrast, the concentrations of nucleation-mode particles were very low. For
300 example, the concentration of N_{NUC} ranged from 1 to 38 cm^{-3} with an average of $8 \pm 4 \text{ cm}^{-3}$. We also
301 observed $\text{CN}_{2.5}$ values at the background level of $\sim 460 \pm 70 \text{ cm}^{-3}$, which are consistent with the
302 measurements collected at a coastal Antarctic station during summer ($\sim 600 \text{ cm}^{-3}$) (Kim et al., 2017) and
303 from flight-based measurements over the Arctic Ocean ($\sim 300 \text{ cm}^{-3}$) (Burkart et al., 2017).

304

305 **3.3. Overview of aerosol properties according to different air mass back trajectories**

306 Air masses comprising marine Pacific along with marine and terrestrial Arctic air masses were
307 encountered during the campaign. In the section 3.2, two case studies of NPF events (Fig. 4 and Fig. 5)
308 were found in the Arctic atmosphere. As stressed in Willis et al., (2018), NPF and growth is frequently
309 observed in the boundary layer in the both Arctic open ocean and coastal regions. These events seem to
310 occur more frequently than lower-latitude marine boundary layers (Quinn and Bates, 2011); there are
311 multiple reasons including summer 24-h high solar radiation, low condensation sink, low temperature
312 and low mixing of surface emissions, as recently reviewed in Abbatt et al. (2019). Our study also
313 confirmed that any NPF was not detected during the Pacific transect.

314 In this section, we present an overall meteorological air mass summary of the open ocean field study,
315 categorizing it into three synoptic period types: Pacific marine, Arctic marine and Arctic terrestrial.



316 These classifications do not represent specific air mass back trajectories analysis, but they can mainly
317 represent air masses that have been travelled over these three distinct geographical regions (section 2.4).
318 Average size distributions for the three selected periods in the different air masses are shown in Fig. 7.
319 In addition, a summary of total number concentrations of particles for these periods is included in Table
320 1.

321
322 - *Arctic Marine*. A trimodal distribution was seen at 18 ± 3 nm, 53 ± 6 nm and 150 ± 6 nm. The first
323 mode is due to NPF arriving from open pack sea ice and open ocean Arctic regions, as discussed in
324 Section 3.2.1 where a case study is presented. The Aitken mode (~ 53 nm) is remarkably similar to the
325 Pacific Ocean aerosol size distribution and to previous studies detected in the Arctic regions (Tunved et
326 al., 2013; Freud et al., 2017; Dall'Osto et al., 2019). The largest mode at ~ 150 nm may be due to a
327 combination of primary and secondary aerosol components.

328
329 - *Arctic terrestrial*. A bimodal distribution is seen with two main modes at 24 ± 3 nm and 151 ± 3 nm,
330 respectively. The nucleation and Aitken modes are much higher than the accumulation mode, suggesting
331 that NPF governs the aerosol processes in this coastal region at this time of the year.

332
333 - *Pacific marine*. The Pacific Ocean aerosol size distributions showed a trimodal size distribution at 56
334 ± 3 nm, 130 ± 3 nm and 220 ± 6 nm. The lowest peak at ~ 56 nm (i.e., Aitken mode) is likely a
335 combination of primary and secondary marine aerosol components, whereas the largest peak at ~ 220
336 nm might be caused by cloud processing and aged aerosols. The mode at ~ 130 nm could originate from
337 primary sea spray aerosols in the Pacific atmosphere (Quinn et al., 2015). When the distribution is fitted
338 with log-normal modes, the inter-modal minimum is calculated to be ~ 120 nm - often known as Hoppel
339 minimum as a signature of cloud processing (Hoppel et al., 1994) - although, it is difficult to draw a
340 firm conclusion due to the overlap with the third mode at ~ 130 nm.

341
342 This study shows that aerosol originating from higher and lower marine latitudes – although both



343 being treated as marine air masses - have very different features, as pointed out in several previous
344 studies (Dall'Osto et al., 2010;Frossard et al., 2014). A key conclusion of this study is that we also need
345 to separate different bioregions in the Arctic, especially given the current results showing very different
346 aerosol size distributions in the Arctic study areas (Fig. 7; Arctic marine and Arctic terrestrial). The
347 reasons for the much higher aerosol concentrations near the coast of Alaska relative to the open ocean
348 sympagic and pelagic regions may be multiple. We discuss at least two major sources may contribute to
349 the high aerosol concentrations recorded.

350 The first source of aerosols in the terrestrial Arctic air masses may be due to anthropogenic sources.
351 Due to sea ice retreat and better technologies, the Arctic is now easily accessible to human activities,
352 including oil and gas extraction (Law and Stohl, 2007;Peters et al., 2011). These Arctic oil fields can
353 emit the large amounts of aerosols, and with on-going Arctic development, such local combustion
354 emissions may increase in the future, possibly affecting local air quality (Gunsch et al., 2017;Schmale et
355 al., 2018a). In fact, some NPF events were reported within the North Slope of Alaska (e.g., Prudhoe Bay
356 oil fields) during August and September 2016 at Oliktok Point Alaska. This observation was suggested
357 to be linked with oil fields emissions (Kolesar et al., 2017). However, our measurements were
358 conducted in the open ocean, quite far from any land oil field local emissions. BC data were collected as
359 shown in Fig. 8; they revealed very high standard deviations due to high detection limit of the
360 instrument used relative to the concentrations detected. However, no remarkable differences can be seen,
361 all pointing to pristine clean marine air masses with BC values of approximately $20 \pm 10 \text{ ng m}^{-3}$. The
362 two Arctic categories (Marine and Terrestrial) shows similar BC values, whereas higher values can be
363 seen for the Pacific marine aerosol category, probably due to contamination from nearby Asian high
364 pollutant sources.

365 The second source of aerosol in the terrestrial Arctic air masses may be due to terrestrial natural
366 sources. We believe that this may be a much more probable reason. The Arctic Ocean is submerged
367 under areas of relatively shallow water known as a shelf sea for ~50% of its area. It is a relatively small
368 ocean, characterized by pronounced riverine influence and a complex hydrography. Up to 11% of the



369 entire global river discharge ends up in the Arctic Ocean (Shiklomanov et al., 2000), which is only 1%
370 of the global ocean volume. The discharge of freshwater is increasing (Peterson et al., 2002), impacting
371 coastal salinity and carbon cycle. Indeed, this continental runoff is a major source of freshwater,
372 nutrients and terrigenous material to the Arctic Ocean (Benner et al., 2005;Fichot et al., 2013;Massicotte
373 et al., 2017). The warming climate in the region is causing permafrost degradation, alterations to
374 regional hydrology and shifting amounts and composition of dissolved organic matter (DOM)
375 transported by streams and rivers (Mann et al., 2016;Chen et al., 2017). Overall, there is a considerable
376 spatial and temporal heterogeneity in the distribution of the DOC in the Arctic, owing to strong
377 biological and physicochemical processes. It is important to remember that sea ice formation and
378 melting also affects the concentrations and distributions of DOC, although its impact is still difficult to
379 resolve (Fichot et al., 2013;Shen et al., 2012).

380 In a recent paper (Park et al., 2019), we suggested that the large amount of freshwater from river
381 runoff may have a substantial impact on primary aerosol production mechanisms, possibly affecting the
382 cloud radiative forcing. We showed that the Arctic riverine organic matter can be directly emitted from
383 surface seawater into the atmosphere via bubble bursting (Park et al., 2019). The high amount of DOC
384 populating the sea-surface microlayer (SML) in the Arctic waters - including UV absorbing humic
385 substances - can also produce VOCs (Ciuraru et al., 2015;Fu et al., 2015), which are known precursors
386 of secondary organic aerosols. Recently, Mungall et al. (2017) reported that the marine microlayer in the
387 Canadian Arctic Archipelago is a source of oxidized VOCs (OVOCs), which could be an important
388 source of biogenic secondary organic aerosol (Croft et al., 2019). Previous studies also reported
389 fluorescent water-soluble organic aerosols in the High Arctic atmosphere (Fu et al., 2015). It is worth
390 noting that terrestrial VOCs from tundra and lakes at elevated concentrations were reported (Potosnak et
391 al., 2013;Lindwall et al., 2016;Steinke et al., 2018).

392 Fig. 9 shows DOC concentrations from water samples taken in the areas where the NPF marine and
393 terrestrial case studies (Section 3.2.1 and 3.2.2) were detected. It is clear that as much as twice higher
394 concentrations are seen for the coastal marine areas, relative to the open ocean marine regions. The



395 origin of this organic matter can be obtained by the FDOM analysis. Fig. 9 (bottom) shows specific
396 peaks attributed to different chemical features. The ratio of terrestrial humic substances (peak A) was
397 3.5 for the terrestrial/marine samples. By striking contrast, marine fulvic substances (peak M) and
398 proteinaceous (peak T) had a ratio of 0.45 and 0.27, respectively, showing two very distinct chemical
399 compounds. This suggests that coastal oceanic water enriched in river organic material as well as fresh
400 water tundra and lake may be a source of VOC (both from biotic and abiotic emission processes) that
401 may be responsible for the high secondary aerosols detected near these areas.

402

403 **3.4. Impact on CCN number concentrations**

404 Fig. 10a illustrates the CCN concentrations for the three selected periods under different
405 supersaturation conditions. For a given SS of 0.4%, CCN concentrations for Arctic marine, Arctic
406 terrestrial and Pacific marine air masses were $35 \pm 40 \text{ cm}^{-3}$, $71 \pm 47 \text{ cm}^{-3}$, and $204 \pm 87 \text{ cm}^{-3}$,
407 respectively. Higher concentrations of CCN were observed when the air mass originated from the
408 Pacific marine for a SS of 0.2%–1.0 %. This may have occurred due to the differences in the CCN
409 sources between the Arctic and Pacific Oceans. It was noted that that accumulation and coarse-mode
410 particles, which are predominant over the Pacific Ocean (Fig. 7), can easily act as CCN. Our results
411 agreed well with values reported in previous studies that measured CCN at a ground-based Arctic
412 station (Jung et al., 2018), but was slightly higher than those measured from high-Arctic expeditions
413 (Leck et al., 2002; Martin et al., 2011; Mauritsen et al., 2011). For example, Jung et al. (2018) reported
414 seasonal variations in the CCN concentration over seven years (2007–2013) at the Zeppelin station, and
415 found that the monthly mean CCN concentrations ranged from 17 cm^{-3} in October 2007 to 198 cm^{-3} in
416 March 2008 at a SS value of 0.4%. However, Mauritsen et al. (2011) observed CCN concentrations
417 lower than $\sim 100 \text{ cm}^{-3}$ at five different supersaturations (SS = 0.10%, 0.15%, 0.20%, 0.41%, and 0.73%),
418 with median values ranging from 15 to 50 cm^{-3} , in four High Arctic expeditions during the Arctic
419 Summer Cloud Ocean Study. Such values were also in line with the long term measurement at an Arctic
420 station in Barrow, which indicated that the median CCN concentrations at 0.2% SS was smaller than



421 100 cm^{-3} (Schmale et al., 2018b).

422 We also compared CCN activity and critical diameter for the three selected periods, as shown in Fig.
423 10b and c. The CCN activity is defined as the ratio of the number concentration of particles that
424 activated to become CCN at a given supersaturation to the total number concentration of particles larger
425 than 2.5 nm ($\text{CN}_{2.5}$). The CCN activity followed a similar pattern as the CCN concentration.
426 Furthermore, the critical diameter (D_c) was estimated using the measured aerosol size distribution,
427 $\text{CN}_{2.5}$, and CCN concentrations with a time resolution of 1 h, as described by Furutani et al., (2014).
428 The D_c at a SS of 0.4% was found to be 103 ± 43 nm, 83 ± 18 nm, and 136 ± 67 nm for Arctic marine,
429 Arctic terrestrial, and Pacific marine periods, respectively. These values are comparable to previous
430 studies obtained in the Arctic and subarctic regions. For instance, Jaatinen et al. (2014) reported that the
431 D_c value of 98 ± 16 nm (SS = 0.4%) from the subarctic area of Finland (Pallas-Sodankylä Global
432 Atmospheric Watch station). Anttila et al. (2012) also showed that a D_c value was in the range of 90 to
433 120 nm at a SS of 0.4% during the same field campaign as reported in Jaatinen et al. (2014). For a
434 maximum SS between 0.18 and 0.26%, D_c varied between 110 and 140 nm at the same measurement
435 sites.

436

437 **4. Summary and conclusions**

438 This study presents the physical properties of aerosol particles measured aboard the R/V Araon ice-
439 breaker during 2017 throughout the Arctic and Pacific Oceans. The $\text{CN}_{2.5}$ value commonly ranged
440 between 13 and $2,000 \text{ cm}^{-3}$ with an average of $505 \pm 280 \text{ cm}^{-3}$. An elevated $\text{CN}_{2.5}$ concentration
441 reaching $\sim 6,016 \text{ cm}^{-3}$ was observed from 13 September to 20 September. The temporal variations in the
442 $\text{CN}_{2.5}$ concentration followed a similar pattern to those of N_{NUA} and N_{AIT} . We also found that the $\text{CN}_{2.5}$
443 concentration was strongly correlated with N_{NUA} ($r^2 = 0.69$), suggesting that CN was mainly derived
444 from nucleation-mode particles.

445 NPF events caused by gas-to-particle conversion frequently occurred over the Arctic Ocean.

446 Overall, two major NPF sources (i.e., Arctic marine and Arctic terrestrial) were identified based on the



447 backward air mass trajectory analysis. NPF events were associated with Arctic marine air masses,
448 indicating the impact of marine biogenic emissions from the Arctic Ocean. Strong NPF events with
449 particle growth were associated with Arctic terrestrial air masses, which may be due to the biogenic
450 precursor gases emitted by terrestrial ecosystems including river discharge and Alaskan tundra in the
451 Arctic coastal areas. In contrast, relatively larger particles with broad Aitken and accumulation-mode
452 peaks were observed over the Pacific Ocean. Our study confirmed that any NPF was not detected during
453 the Pacific transect. We also compared the average CCN concentrations for each of the cases. Our data
454 showed that the impact of aerosols on CCN concentrations ($SS = 0.4\%$) was significant: $35 \pm 40 \text{ cm}^{-3}$,
455 $71 \pm 47 \text{ cm}^{-3}$, and $204 \pm 87 \text{ cm}^{-3}$ for Arctic marine, Arctic terrestrial, and Pacific marine periods,
456 respectively. Our interpreted data showed that river outflows and tundra strongly influence Arctic
457 aerosol properties. Further detailed measurements of the chemical characteristics of marine aerosols are
458 required to provide more direct evidence for the contribution of biogenic precursors to the NPF and
459 CCN in the remote Arctic atmosphere.

460 Arctic areas are currently experiencing drastic climate change, with air temperatures increasing at
461 twice the rate of the global average. This warming is causing clear changes, such as the increases in
462 biogenic emissions from tundra vegetation and changes in vegetation cover (Faubert et al.,
463 2010;Peñuelas and Staudt, 2010;Potosnak et al., 2013;Lindwall et al., 2016). Lindwall et al. (2016)
464 observed a 280% increase in VOC emissions relative to the ambient level in response to a 4 °C increase
465 in the summer temperature of the Subarctic. Increases in VOC emissions from river discharge and
466 tundra vegetation in the Arctic are critical factors that induce NPF and particle growth events, which
467 may impact the CCN concentrations during the Arctic summer.

468

469 **Data availability**

470 The data analyzed in this publication will be readily provided upon request to the corresponding author
471 (yjyoon@kopri.re.kr).

472

473 **Author contributions**



474 JP, YJY designed the study, JP, MD'O, KP, YG, HJK, EJ, KTP, MP, SSY, JJ, and BYL analyzed data.
475 JP, MD'O, KTP and YJY prepared the manuscript with contributions from all co-authors.

476

477 **Competing interests**

478 The authors declare that they have no conflict of interest.

479

480 **Acknowledgements**

481 We are grateful to the captain and crews of R/V *Araon* for their enthusiastic assistance during the cruise
482 of ARA08C. This work was supported by a Korea Grant from the Korean Government (MSIP) (NRF-
483 2016M1A5A1901769) (KOPRI-PN19081) and the KOPRI projects (PE17390). Kihong Park was
484 supported by the National Leading Research Laboratory program (NRF-2019R1A2C3007202). Minsu
485 Park and Seong Soo Yum were supported by National Research Foundation of Korea (NRF) grant
486 (NRF-20180R1A2B2006965). Jinyoung Jung was supported by “Korea-Arctic Ocean Observing
487 System (K-AOOS)”, KOPRI, 20160245, funded by the MOF, Korea.

488

489 **References**

- 490 Abbatt, J. P. D., Leaitch, W. R., Aliabadi, A. A., Bertram, A. K., Blanchet, J. P., Boivin-Rioux, A.,
491 Bozem, H., Burkart, J., Chang, R. Y. W., Charette, J., Chaubey, J. P., Christensen, R. J., Cirisan,
492 A., Collins, D. B., Croft, B., Dionne, J., Evans, G. J., Fletcher, C. G., Galí, M.,
493 Ghahremaninezhad, R., Girard, E., Gong, W., Gosselin, M., Gourdal, M., Hanna, S. J.,
494 Hayashida, H., Herber, A. B., Hesaraki, S., Hoor, P., Huang, L., Hussherr, R., Irish, V. E., Keita,
495 S. A., Kodros, J. K., Köllner, F., Kolonjari, F., Kunkel, D., Ladino, L. A., Law, K., Lévasseur, M.,
496 Libois, Q., Liggio, J., Lizotte, M., Macdonald, K. M., Mahmood, R., Martin, R. V., Mason, R. H.,
497 Miller, L. A., Moravek, A., Mortenson, E., Mungall, E. L., Murphy, J. G., Namazi, M., Norman,
498 A. L., O'Neill, N. T., Pierce, J. R., Russell, L. M., Schneider, J., Schulz, H., Sharma, S., Si, M.,
499 Staebler, R. M., Steiner, N. S., Thomas, J. L., von Salzen, K., Wentzell, J. J. B., Willis, M. D.,
500 Wentworth, G. R., Xu, J. W., and Yakobi-Hancock, J. D.: Overview paper: New insights into
501 aerosol and climate in the Arctic, *Atmos. Chem. Phys.*, 19, 2527-2560, 10.5194/acp-19-2527-
502 2019, 2019.
- 503 ACIA: Arctic Climate Impact Assessment, chap. 2, p. 23, Cambridge University Press, New York, USA,,
504 2005.
- 505 Allan, J. D., Williams, P. I., Najera, J., Whitehead, J. D., Flynn, M. J., Taylor, J. W., Liu, D., Darbyshire,
506 E., Carpenter, L. J., Chance, R., Andrews, S. J., Hackenberg, S. C., and McFiggans, G.: Iodine
507 observed in new particle formation events in the Arctic atmosphere during ACCACIA, *Atmos.*
508 *Chem. Phys.*, 15, 5599-5609, 10.5194/acp-15-5599-2015, 2015.
- 509 Asmi, E., Kondratyev, V., Brus, D., Laurila, T., Lihavainen, H., Backman, J., Vakkari, V., Aurela, M.,
510 Hatakka, J., Viisanen, Y., Uttal, T., Ivakhov, V., and Makshtas, A.: Aerosol size distribution
511 seasonal characteristics measured in Tiksi, Russian Arctic, *Atmos. Chem. Phys.*, 16, 1271-1287,
512 10.5194/acp-16-1271-2016, 2016.



- 513 Benner, R., Louchouart, P., and Amon, R. M. W.: Terrigenous dissolved organic matter in the Arctic
514 Ocean and its transport to surface and deep waters of the North Atlantic, *Global Biogeochemical*
515 *Cycles*, 19, doi:10.1029/2004GB002398, 2005.
- 516 Burkart, J., Willis, M. D., Bozem, H., Thomas, J. L., Law, K., Hoor, P., Aliabadi, A. A., Köllner, F.,
517 Schneider, J., Herber, A., Abbatt, J. P. D., and Leaitch, W. R.: Summertime observations of
518 elevated levels of ultrafine particles in the high Arctic marine boundary layer, *Atmos. Chem.*
519 *Phys.*, 17, 5515-5535, 10.5194/acp-17-5515-2017, 2017.
- 520 Chang, R. Y.-W., Sjostedt, S. J., Pierce, J. R., Papayriakou, T. N., Scarratt, M. G., Michaud, S.,
521 Levasseur, M., Leaitch, W. R., and Abbatt, J. P. D.: Relating atmospheric and oceanic DMS
522 levels to particle nucleation events in the Canadian Arctic, *Journal of Geophysical Research:*
523 *Atmospheres*, 116, doi:10.1029/2011JD015926, 2011.
- 524 Chen, X., Zhang, X., Church, J. A., Watson, C. S., King, M. A., Monselesan, D., Legresy, B., and Harig,
525 C.: The increasing rate of global mean sea-level rise during 1993–2014, *Nature Climate Change*,
526 7, 492, 10.1038/nclimate3325 [https://www.nature.com/articles/nclimate3325#supplementary-](https://www.nature.com/articles/nclimate3325#supplementary-information)
527 [information](https://www.nature.com/articles/nclimate3325#supplementary-information), 2017.
- 528 Ciuraru, R., Fine, L., van Pinxteren, M., D'Anna, B., Herrmann, H., and George, C.: Photosensitized
529 production of functionalized and unsaturated organic compounds at the air-sea interface,
530 *Scientific Reports*, 5, 12741, 10.1038/srep12741
531 <https://www.nature.com/articles/srep12741#supplementary-information>, 2015.
- 532 Coble, P. G.: Marine Optical Biogeochemistry: The Chemistry of Ocean Color, *Chemical Reviews*, 107,
533 402-418, 10.1021/cr050350+, 2007.
- 534 Croft, B., Martin, R. V., Leaitch, W. R., Tunved, P., Breider, T. J., D'Andrea, S. D., and Pierce, J. R.:
535 Processes controlling the annual cycle of Arctic aerosol number and size distributions, *Atmos.*
536 *Chem. Phys.*, 16, 3665-3682, 10.5194/acp-16-3665-2016, 2016.
- 537 Croft, B., Martin, R. V., Leaitch, W. R., Burkart, J., Chang, R. Y. W., Collins, D. B., Hayes, P. L.,
538 Hodshire, A. L., Huang, L., Kodros, J. K., Moravek, A., Mungall, E. L., Murphy, J. G., Sharma,
539 S., Tremblay, S., Wentworth, G. R., Willis, M. D., Abbatt, J. P. D., and Pierce, J. R.: Arctic
540 marine secondary organic aerosol contributes significantly to summertime particle size
541 distributions in the Canadian Arctic Archipelago, *Atmos. Chem. Phys.*, 19, 2787-2812,
542 10.5194/acp-19-2787-2019, 2019.
- 543 Dall'Osto, M., Ceburnis, D., Martucci, G., Bialek, J., Dupuy, R., Jennings, S. G., Berresheim, H.,
544 Wenger, J., Healy, R., Facchini, M. C., Rinaldi, M., Giulianelli, L., Finessi, E., Worsnop, D., Ehn,
545 M., Mikkilä, J., Kulmala, M., and O'Dowd, C. D.: Aerosol properties associated with air masses
546 arriving into the North East Atlantic during the 2008 Mace Head EUCAARI intensive observing
547 period: an overview, *Atmos. Chem. Phys.*, 10, 8413-8435, 10.5194/acp-10-8413-2010, 2010.
- 548 Dall'Osto, M., Beddows, D. C. S., Tunved, P., Harrison, R. M., Lupi, A., Vitale, V., Becagli, S., Traversi,
549 R., Park, K. T., Yoon, Y. J., Massling, A., Skov, H., Lange, R., Strom, J., and Krejci, R.:
550 Simultaneous measurements of aerosol size distributions at three sites in the European high
551 Arctic, *Atmos. Chem. Phys.*, 19, 7377-7395, 10.5194/acp-19-7377-2019, 2019.
- 552 Dall'Osto, M., Beddows, D. C. S., Tunved, P., Krejci, R., Ström, J., Hansson, H. C., Yoon, Y. J., Park,
553 K.-T., Becagli, S., Udisti, R., Onasch, T., O'Dowd, C. D., Simó, R., and Harrison, R. M.: Arctic
554 sea ice melt leads to atmospheric new particle formation, *Scientific Reports*, 7, 3318,
555 10.1038/s41598-017-03328-1, 2017.
- 556 Ehn, M., Vuollekoski, H., Petäjä, T., Kerminen, V.-M., Vana, M., Aalto, P., de Leeuw, G., Ceburnis, D.,
557 Dupuy, R., O'Dowd, C. D., and Kulmala, M.: Growth rates during coastal and marine new
558 particle formation in western Ireland, *Journal of Geophysical Research: Atmospheres*, 115,
559 doi:10.1029/2010JD014292, 2010.
- 560 Faubert, P., Tiiva, P., Rinnan, Å., Michelsen, A., Holopainen, J. K., and Rinnan, R.: Doubled volatile
561 organic compound emissions from subarctic tundra under simulated climate warming, 187, 199-
562 208, 10.1111/j.1469-8137.2010.03270.x, 2010.
- 563 Fichot, C. G., Kaiser, K., Hooker, S. B., Amon, R. M. W., Babin, M., Bélanger, S., Walker, S. A., and



- 564 Benner, R.: Pan-Arctic distributions of continental runoff in the Arctic Ocean, *Scientific Reports*,
565 3, 1053, 10.1038/srep01053 <https://www.nature.com/articles/srep01053#supplementary->
566 information, 2013.
- 567 Freud, E., Krejci, R., Tunved, P., Leaitch, R., Nguyen, Q. T., Massling, A., Skov, H., and Barrie, L.:
568 Pan-Arctic aerosol number size distributions: seasonality and transport patterns, *Atmos. Chem.*
569 *Phys.*, 17, 8101-8128, 10.5194/acp-17-8101-2017, 2017.
- 570 Frossard, A. A., Russell, L. M., Burrows, S. M., Elliott, S. M., Bates, T. S., and Quinn, P. K.: Sources
571 and composition of submicron organic mass in marine aerosol particles, 119, 12,977-913,003,
572 10.1002/2014jd021913, 2014.
- 573 Fu, P., Kawamura, K., Chen, J., Qin, M., Ren, L., Sun, Y., Wang, Z., Barrie, L. A., Tachibana, E., Ding,
574 A., and Yamashita, Y.: Fluorescent water-soluble organic aerosols in the High Arctic atmosphere,
575 *Scientific Reports*, 5, 9845, 10.1038/srep09845, 2015.
- 576 Gunsch, M. J., Kirpes, R. M., Kolesar, K. R., Barrett, T. E., China, S., Sheesley, R. J., Laskin, A.,
577 Wiedensohler, A., Tuch, T., and Pratt, K. A.: Contributions of transported Prudhoe Bay oil field
578 emissions to the aerosol population in Utqiagvik, Alaska, *Atmos. Chem. Phys.*, 17, 10879-10892,
579 10.5194/acp-17-10879-2017, 2017.
- 580 Heintzenberg, J., Leck, C., and Tunved, P.: Potential source regions and processes of aerosol in the
581 summer Arctic, *Atmos. Chem. Phys.*, 15, 6487-6502, 10.5194/acp-15-6487-2015, 2015.
- 582 Heintzenberg, J., Tunved, P., Galí, M., and Leck, C.: New particle formation in the Svalbard region
583 2006–2015, *Atmos. Chem. Phys.*, 17, 6153-6175, 10.5194/acp-17-6153-2017, 2017.
- 584 Hoppel, W. A., Frick, G. M., Fitzgerald, J. W., and Larson, R. E.: Marine boundary layer measurements
585 of new particle formation and the effects nonprecipitating clouds have on aerosol size
586 distribution, 99, 14443-14459, 10.1029/94jd00797, 1994.
- 587 Hudson, J. G., and Yum, S. S.: Cloud condensation nuclei spectra and polluted and clean clouds over the
588 Indian Ocean, 107, INX2 21-21-INX22 21-12, 10.1029/2001jd000829, 2002.
- 589 IPCC: Climate change 2013: The physical science basis, Intergovernmental panel on Climate Change,
590 Cambridge University Press, New York, USA, 571-740, 2013.
- 591 Jang, E., Park, K. T., Yoon, Y. J., Kim, T. W., Hong, S. B., Becagli, S., Traversi, R., Kim, J., and Gim,
592 Y.: New particle formation events observed at the King Sejong Station, Antarctic Peninsula –
593 Part 2: Link with the oceanic biological activities, *Atmos. Chem. Phys.*, 19, 7595-7608,
594 10.5194/acp-19-7595-2019, 2019.
- 595 Jung, C. H., Yoon, Y. J., Kang, H. J., Gim, Y., Lee, B. Y., Ström, J., Krejci, R., and Tunved, P.: The
596 seasonal characteristics of cloud condensation nuclei (CCN) in the arctic lower troposphere,
597 *Tellus B: Chemical and Physical Meteorology*, 70, 1-13, 10.1080/16000889.2018.1513291, 2018.
- 598 Kalivitis, N., Kerminen, V. M., Kouvarakis, G., Stavroulas, I., Bougiatioti, A., Nenes, A., Manninen, H.
599 E., Petäjä, T., Kulmala, M., and Mihalopoulos, N.: Atmospheric new particle formation as a
600 source of CCN in the eastern Mediterranean marine boundary layer, *Atmos. Chem. Phys.*, 15,
601 9203-9215, 10.5194/acp-15-9203-2015, 2015.
- 602 Kerminen, V.-M., Chen, X., Vakkari, V., Petäjä, T., Kulmala, M., and Bianchi, F.: Atmospheric new
603 particle formation and growth: review of field observations, *Environmental Research Letters*, 13,
604 103003, 10.1088/1748-9326/aadf3c, 2018.
- 605 Kim, G., Cho, H.-j., Seo, A., Kim, D., Gim, Y., Lee, B. Y., Yoon, Y. J., and Park, K.: Comparison of
606 Hygroscopicity, Volatility, and Mixing State of Submicrometer Particles between Cruises over
607 the Arctic Ocean and the Pacific Ocean, *Environmental Science & Technology*, 49, 12024-12035,
608 10.1021/acs.est.5b01505, 2015.
- 609 Kim, J., Yoon, Y. J., Gim, Y., Kang, H. J., Choi, J. H., Park, K. T., and Lee, B. Y.: Seasonal variations in
610 physical characteristics of aerosol particles at the King Sejong Station, Antarctic Peninsula,
611 *Atmos. Chem. Phys.*, 17, 12985-12999, 10.5194/acp-17-12985-2017, 2017.
- 612 Kim, J., Yoon, Y. J., Gim, Y., Choi, J. H., Kang, H. J., Park, K. T., Park, J., and Lee, B. Y.: New particle
613 formation events observed at King Sejong Station, Antarctic Peninsula – Part 1: Physical



- 614 characteristics and contribution to cloud condensation nuclei, *Atmos. Chem. Phys.*, 19, 7583-
615 7594, 10.5194/acp-19-7583-2019, 2019.
- 616 Kolesar, K. R., Cellini, J., Peterson, P. K., Jefferson, A., Tuch, T., Birmili, W., Wiedensohler, A., and
617 Pratt, K. A.: Effect of Prudhoe Bay emissions on atmospheric aerosol growth events observed in
618 Utqiagvik (Barrow), Alaska, *Atmospheric Environment*, 152, 146-155,
619 <https://doi.org/10.1016/j.atmosenv.2016.12.019>, 2017.
- 620 Kulmala, M., Vehkamäki, H., Petäjä, T., Dal Maso, M., Lauri, A., Kerminen, V. M., Birmili, W., and
621 McMurry, P. H.: Formation and growth rates of ultrafine atmospheric particles: a review of
622 observations, *Journal of Aerosol Science*, 35, 143-176,
623 <https://doi.org/10.1016/j.jaerosci.2003.10.003>, 2004.
- 624 Law, K. S., and Stohl, A.: Arctic Air Pollution: Origins and Impacts, *Science*, 315, 1537-1540,
625 10.1126/science.1137695, 2007.
- 626 Leaitch, W. R., Sharma, S., Huang, L., Toom-Saunty, D., Chivulescu, A., Macdonald, A. M., von
627 Salzen, K., Pierce, J. R., Bertram, A. K., Schroder, J. C., Shantz, N. C., Chang, R. Y.-W., and
628 Norman, A.-L.: Dimethyl sulfide control of the clean summertime Arctic aerosol and cloud,
629 *Elem. Sci. Anth.*, 1, 000017, 10.12952/journal.elementa.000017, 2013.
- 630 Leck, C., Norman, M., Bigg, E. K., and Hillamo, R.: Chemical composition and sources of the high
631 Arctic aerosol relevant for cloud formation, 107, *AAC 1-1-AAC 1-17*, 10.1029/2001jd001463,
632 2002.
- 633 Levasseur, M.: Impact of Arctic meltdown on the microbial cycling of sulphur, *Nature Geoscience*, 6,
634 691, 10.1038/ngeo1910, 2013.
- 635 Lindwall, F., Schollert, M., Michelsen, A., Blok, D., and Rinnan, R.: Fourfold higher tundra volatile
636 emissions due to arctic summer warming, 121, 895-902, 10.1002/2015jg003295, 2016.
- 637 Mann, P. J., Spencer, R. G. M., Hernes, P. J., Six, J., Aiken, G. R., Tank, S. E., McClelland, J. W., Butler,
638 K. D., Dyda, R. Y., and Holmes, R. M.: Pan-Arctic Trends in Terrestrial Dissolved Organic
639 Matter from Optical Measurements, 4, 10.3389/feart.2016.00025, 2016.
- 640 Martin, M., Chang, R. Y. W., Sierau, B., Sjogren, S., Swietlicki, E., Abbatt, J. P. D., Leck, C., and
641 Lohmann, U.: Cloud condensation nuclei closure study on summer arctic aerosol, *Atmos. Chem.*
642 *Phys.*, 11, 11335-11350, 10.5194/acp-11-11335-2011, 2011.
- 643 Massicotte, P., Asmala, E., Stedmon, C., and Markager, S.: Global distribution of dissolved organic
644 matter along the aquatic continuum: Across rivers, lakes and oceans, *Science of The Total*
645 *Environment*, 609, 180-191, <https://doi.org/10.1016/j.scitotenv.2017.07.076>, 2017.
- 646 Mauritsen, T., Sedlar, J., Tjernström, M., Leck, C., Martin, M., Shupe, M., Sjogren, S., Sierau, B.,
647 Persson, P. O. G., Brooks, I. M., and Swietlicki, E.: An Arctic CCN-limited cloud-aerosol regime,
648 *Atmos. Chem. Phys.*, 11, 165-173, 10.5194/acp-11-165-2011, 2011.
- 649 Merikanto, J., Spracklen, D. V., Mann, G. W., Pickering, S. J., and Carslaw, K. S.: Impact of nucleation
650 on global CCN, *Atmos. Chem. Phys.*, 9, 8601-8616, 10.5194/acp-9-8601-2009, 2009.
- 651 Mungall, E. L., Croft, B., Lizotte, M., Thomas, J. L., Murphy, J. G., Levasseur, M., Martin, R. V.,
652 Wentzell, J. J. B., Liggio, J., and Abbatt, J. P. D.: Dimethyl sulfide in the summertime Arctic
653 atmosphere: measurements and source sensitivity simulations, *Atmos. Chem. Phys.*, 16, 6665-
654 6680, 10.5194/acp-16-6665-2016, 2016.
- 655 Németh, Z., and Salma, I.: Spatial extension of nucleating air masses in the Carpathian Basin, *Atmos.*
656 *Chem. Phys.*, 14, 8841-8848, 10.5194/acp-14-8841-2014, 2014.
- 657 Nguyen, Q. T., Glasius, M., Sørensen, L. L., Jensen, B., Skov, H., Birmili, W., Wiedensohler, A.,
658 Kristensson, A., Nøjgaard, J. K., and Massling, A.: Seasonal variation of atmospheric particle
659 number concentrations, new particle formation and atmospheric oxidation capacity at the high
660 Arctic site Villum Research Station, Station Nord, *Atmos. Chem. Phys.*, 16, 11319-11336,
661 10.5194/acp-16-11319-2016, 2016.
- 662 O'Dowd, C., Ceburnis, D., Ovadnevaite, J., Vaishya, A., Rinaldi, M., and Facchini, M. C.: Do
663 anthropogenic, continental or coastal aerosol sources impact on a marine aerosol signature at
664 Mace Head?, *Atmos. Chem. Phys.*, 14, 10687-10704, 10.5194/acp-14-10687-2014, 2014.



- 665 O'Dowd, C. D., Jimenez, J. L., Bahreini, R., Flagan, R. C., Seinfeld, J. H., Hämeri, K., Pirjola, L.,
666 Kulmala, M., Jennings, S. G., and Hoffmann, T.: Marine aerosol formation from biogenic iodine
667 emissions, *Nature*, 417, 632, 10.1038/nature00775, 2002.
- 668 Oziel, L., Neukermans, G., Ardyna, M., Lancelot, C., Tison, J.-L., Wassmann, P., Sirven, J., Ruiz-Pino,
669 D., and Gascard, J.-C.: Role for Atlantic inflows and sea ice loss on shifting phytoplankton
670 blooms in the Barents Sea, 122, 5121-5139, 10.1002/2016jc012582, 2017.
- 671 Pang, X., Pu, J., Zhao, X., Ji, Q., Qu, M., and Cheng, Z.: Comparison between AMSR2 Sea Ice
672 Concentration Products and Pseudo-Ship Observations of the Arctic and Antarctic Sea Ice Edge
673 on Cloud-Free Days, 10, 317, 2018.
- 674 Park, J., Dall'Osto, M., Park, K., Kim, J.-H., Park, J., Park, K.-T., Hwang, C. Y., Jang, G. I., Gim, Y.,
675 Kang, S., Park, S., Jin, Y. K., Yum, S. S., Simó, R., and Yoon, Y. J.: Arctic Primary Aerosol
676 Production Strongly Influenced by Riverine Organic Matter, *Environmental Science &
677 Technology*, 53, 8621-8630, 10.1021/acs.est.9b03399, 2019.
- 678 Park, K.-T., Lee, K., Kim, T.-W., Yoon, Y. J., Jang, E.-H., Jang, S., Lee, B.-Y., and Hermansen, O.:
679 Atmospheric DMS in the Arctic Ocean and Its Relation to Phytoplankton Biomass, 32, 351-359,
680 10.1002/2017gb005805, 2018.
- 681 Park, K. T., Jang, S., Lee, K., Yoon, Y. J., Kim, M. S., Park, K., Cho, H. J., Kang, J. H., Udusti, R., Lee,
682 B. Y., and Shin, K. H.: Observational evidence for the formation of DMS-derived aerosols
683 during Arctic phytoplankton blooms, *Atmos. Chem. Phys.*, 17, 9665-9675, 10.5194/acp-17-
684 9665-2017, 2017.
- 685 Peñuelas, J., and Staudt, M.: BVOCs and global change, *Trends in Plant Science*, 15, 133-144,
686 <https://doi.org/10.1016/j.tplants.2009.12.005>, 2010.
- 687 Peters, G. P., Nilssen, T. B., Lindholt, L., Eide, M. S., Glomsrød, S., Eide, L. I., and Fuglestad, J. S.:
688 Future emissions from shipping and petroleum activities in the Arctic, *Atmos. Chem. Phys.*, 11,
689 5305-5320, 10.5194/acp-11-5305-2011, 2011.
- 690 Peterson, B. J., Holmes, R. M., McClelland, J. W., Vörösmarty, C. J., Lammers, R. B., Shiklomanov, A.
691 I., Shiklomanov, I. A., and Rahmstorf, S.: Increasing River Discharge to the Arctic Ocean,
692 *Science*, 298, 2171-2173, 10.1126/science.1077445, 2002.
- 693 Pierce, J. R., Leaitch, W. R., Liggio, J., Westervelt, D. M., Wainwright, C. D., Abbatt, J. P. D., Ahlm, L.,
694 Al-Basheer, W., Cziczó, D. J., Hayden, K. L., Lee, A. K. Y., Li, S. M., Russell, L. M., Sjostedt, S.
695 J., Strawbridge, K. B., Travis, M., Vlasenko, A., Wentzell, J. J. B., Wiebe, H. A., Wong, J. P. S.,
696 and Macdonald, A. M.: Nucleation and condensational growth to CCN sizes during a sustained
697 pristine biogenic SOA event in a forested mountain valley, *Atmos. Chem. Phys.*, 12, 3147-3163,
698 10.5194/acp-12-3147-2012, 2012.
- 699 Potosnak, M. J., Baker, B. M., LeSturgeon, L., Disher, S. M., Griffin, K. L., Bret-Harte, M. S., and
700 Starr, G.: Isoprene emissions from a tundra ecosystem, *Biogeosciences*, 10, 871-889,
701 10.5194/bg-10-871-2013, 2013.
- 702 Quinn, P. K., and Bates, T. S.: The case against climate regulation via oceanic phytoplankton sulphur
703 emissions, *Nature*, 480, 51-56, 10.1038/nature10580, 2011.
- 704 Quinn, P. K., Collins, D. B., Grassian, V. H., Prather, K. A., and Bates, T. S.: Chemistry and Related
705 Properties of Freshly Emitted Sea Spray Aerosol, *Chemical Reviews*, 115, 4383-4399,
706 10.1021/cr500713g, 2015.
- 707 Raso, A. R. W., Custard, K. D., May, N. W., Tanner, D., Newburn, M. K., Walker, L., Moore, R. J., Huey,
708 L. G., Alexander, L., Shepson, P. B., and Pratt, K. A.: Active molecular iodine photochemistry in
709 the Arctic, *Proceedings of the National Academy of Sciences*, 114, 10053-10058,
710 10.1073/pnas.1702803114, 2017.
- 711 Rose, C., Sellegri, K., Moreno, I., Velarde, F., Ramonet, M., Weinhold, K., Krejci, R., Andrade, M.,
712 Wiedensohler, A., Ginot, P., and Laj, P.: CCN production by new particle formation in the free
713 troposphere, *Atmos. Chem. Phys.*, 17, 1529-1541, 10.5194/acp-17-1529-2017, 2017.
- 714 Schmale, J., Arnold, S. R., Law, K. S., Thorp, T., Anenberg, S., Simpson, W. R., Mao, J., and Pratt, K.
715 A.: Local Arctic Air Pollution: A Neglected but Serious Problem, 6, 1385-1412,



- 716 10.1029/2018ef000952, 2018a.
- 717 Schmale, J., Henning, S., Decesari, S., Henzing, B., Keskinen, H., Sellegri, K., Ovadnevaite, J., Pöhlker,
718 M. L., Brito, J., Bougiatioti, A., Kristensson, A., Kalivitis, N., Stavroulas, I., Carbone, S.,
719 Jefferson, A., Park, M., Schlag, P., Iwamoto, Y., Aalto, P., Äijälä, M., Bukowiecki, N., Ehn, M.,
720 Frank, G., Fröhlich, R., Frumau, A., Herrmann, E., Herrmann, H., Holzinger, R., Kos, G.,
721 Kulmala, M., Mihalopoulos, N., Nenes, A., O'Dowd, C., Petäjä, T., Picard, D., Pöhlker, C.,
722 Pöschl, U., Poulain, L., Prévôt, A. S. H., Swietlicki, E., Andreae, M. O., Artaxo, P., Wiedensohler,
723 A., Ogren, J., Matsuki, A., Yum, S. S., Stratmann, F., Baltensperger, U., and Gysel, M.: Long-
724 term cloud condensation nuclei number concentration, particle number size distribution and
725 chemical composition measurements at regionally representative observatories, *Atmos. Chem.*
726 *Phys.*, 18, 2853–2881, 10.5194/acp-18-2853-2018, 2018b.
- 727 Schollert, M., Burchard, S., Faubert, P., Michelsen, A., and Rinnan, R. J. P. B.: Biogenic volatile organic
728 compound emissions in four vegetation types in high arctic Greenland, 37, 237–249,
729 10.1007/s00300-013-1427-0, 2014.
- 730 Sellegri, K., O'Dowd, C. D., Yoon, Y. J., Jennings, S. G., and Leeuw, G. d.: Surfactants and submicron
731 sea spray generation, *Journal of Geophysical Research: Atmospheres*, 111,
732 doi:10.1029/2005JD006658, 2006.
- 733 Shen, Y., Fichot, C., and Benner, R.: Dissolved organic matter composition and bioavailability reflect
734 ecosystem productivity in the Western Arctic Ocean, 2012.
- 735 Shiklomanov, I. A., Shiklomanov, A. I., Lammers, R. B., Peterson, B. J., and Vorosmarty, C. J.: The
736 Dynamics of River Water Inflow to the Arctic Ocean, in: *The Freshwater Budget of the Arctic*
737 *Ocean*, edited by: Lewis, E. L., Jones, E. P., Lemke, P., Prowse, T. D., and Wadhams, P.,
738 Springer Netherlands, Dordrecht, 281–296, 2000.
- 739 Spracklen, D. V., Carslaw, K. S., Kulmala, M., Kerminen, V.-M., Sihto, S.-L., Riipinen, I., Merikanto, J.,
740 Mann, G. W., Chipperfield, M. P., Wiedensohler, A., Birmili, W., and Lihavainen, H.:
741 Contribution of particle formation to global cloud condensation nuclei concentrations,
742 *Geophysical Research Letters*, 35, doi:10.1029/2007GL033038, 2008.
- 743 Steinke, M., Hodapp, B., Subhan, R., Bell, T. G., and Martin-Creuzburg, D.: Flux of the biogenic
744 volatiles isoprene and dimethyl sulfide from an oligotrophic lake, *Scientific Reports*, 8, 630,
745 10.1038/s41598-017-18923-5, 2018.
- 746 Stier, P., Seinfeld, J. H., Kinne, S., and Boucher, O.: Aerosol absorption and radiative forcing, *Atmos.*
747 *Chem. Phys.*, 7, 5237–5261, 10.5194/acp-7-5237-2007, 2007.
- 748 Stroeve, J. C., Serreze, M. C., Holland, M. M., Kay, J. E., Malanik, J., and Barrett, A. P.: The Arctic's
749 rapidly shrinking sea ice cover: a research synthesis, *Climatic Change*, 110, 1005–1027,
750 10.1007/s10584-011-0101-1, 2012.
- 751 Ström, J., Umegård, J., Tørseth, K., Tunved, P., Hansson, H. C., Holmén, K., Wismann, V., Herber, A.,
752 and König-Langlo, G.: One year of particle size distribution and aerosol chemical composition
753 measurements at the Zeppelin Station, Svalbard, March 2000–March 2001, *Physics and*
754 *Chemistry of the Earth, Parts A/B/C*, 28, 1181–1190, <https://doi.org/10.1016/j.pce.2003.08.058>,
755 2003.
- 756 Suni, T., Kulmala, M., Hirsikko, A., Bergman, T., Laakso, L., Aalto, P. P., Leuning, R., Cleugh, H.,
757 Zegelin, S., Hughes, D., van Gorsel, E., Kitchen, M., Vana, M., Hörrak, U., Mirme, S., Mirme,
758 A., Sevanto, S., Twining, J., and Tadros, C.: Formation and characteristics of ions and charged
759 aerosol particles in a native Australian Eucalypt forest, *Atmos. Chem. Phys.*, 8, 129–139,
760 10.5194/acp-8-129-2008, 2008.
- 761 Svenningsson, B., Arneth, A., Hayward, S., Holst, T., Massling, A., Swietlicki, E., Hirsikko, A.,
762 Junninen, H., Riipinen, I., Vana, M., Maso, M. D., Hussein, T., and Kulmala, M.: Aerosol
763 particle formation events and analysis of high growth rates observed above a subarctic wetland–
764 forest mosaic, *Tellus B: Chemical and Physical Meteorology*, 60, 353–364, 10.1111/j.1600-
765 0889.2008.00351.x, 2008.
- 766 TAPE, K., STURM, M., and RACINE, C.: The evidence for shrub expansion in Northern Alaska and



- 767 the Pan-Arctic, 12, 686-702, 10.1111/j.1365-2486.2006.01128.x, 2006.
- 768 Tunved, P., Ström, J., and Krejci, R.: Arctic aerosol life cycle: linking aerosol size distributions
769 observed between 2000 and 2010 with air mass transport and precipitation at Zeppelin station,
770 Ny-Ålesund, Svalbard, Atmos. Chem. Phys., 13, 3643-3660, 10.5194/acp-13-3643-2013, 2013.
- 771 Twomey, S.: Pollution and the planetary albedo, Atmospheric Environment (1967), 8, 1251-1256,
772 [https://doi.org/10.1016/0004-6981\(74\)90004-3](https://doi.org/10.1016/0004-6981(74)90004-3), 1974.
- 773 Väänänen, R., Kyrö, E. M., Nieminen, T., Kivekäs, N., Junninen, H., Virkkula, A., Dal Maso, M.,
774 Lihavainen, H., Viisanen, Y., Svenningsson, B., Holst, T., Arneth, A., Aalto, P. P., Kulmala, M.,
775 and Kerminen, V. M.: Analysis of particle size distribution changes between three measurement
776 sites in northern Scandinavia, Atmos. Chem. Phys., 13, 11887-11903, 10.5194/acp-13-11887-
777 2013, 2013.
- 778 Vana, M., Kulmala, M., Dal Maso, M., Hörrak, U., and Tamm, E.: Comparative study of nucleation
779 mode aerosol particles and intermediate air ions formation events at three sites, 109,
780 10.1029/2003jd004413, 2004.
- 781 Vehkamäki, H., Dal Maso, M., Hussein, T., Flanagan, R., Hyvärinen, A., Lauros, J., Merikanto, P.,
782 Mönkkönen, M., Pihlatie, K., Salminen, K., Sogacheva, L., Thum, T., Ruuskanen, T. M.,
783 Keronen, P., Aalto, P. P., Hari, P., Lehtinen, K. E. J., Rannik, Ü., and Kulmala, M.: Atmospheric
784 particle formation events at Väriö measurement station in Finnish Lapland 1998-2002, Atmos.
785 Chem. Phys., 4, 2015-2023, 10.5194/acp-4-2015-2004, 2004.
- 786 Wang, M., and Overland, J. E.: A sea ice free summer Arctic within 30 years?, Geophysical Research
787 Letters, 36, doi:10.1029/2009GL037820, 2009.
- 788 Westervelt, D. M., Pierce, J. R., and Adams, P. J.: Analysis of feedbacks between nucleation rate,
789 survival probability and cloud condensation nuclei formation, Atmos. Chem. Phys., 14, 5577-
790 5597, 10.5194/acp-14-5577-2014, 2014.
- 791 Willis, M. D., Burkart, J., Thomas, J. L., Köllner, F., Schneider, J., Bozem, H., Hoor, P. M., Aliabadi, A.
792 A., Schulz, H., Herber, A. B., Leaitch, W. R., and Abbatt, J. P. D.: Growth of nucleation mode
793 particles in the summertime Arctic: a case study, Atmos. Chem. Phys., 7663-7679, 10.5194/acp-
794 16-7663-2016, 2016.
- 795 Willis, M. D., Leaitch, W. R., and Abbatt, J. P. D.: Processes Controlling the Composition and
796 Abundance of Arctic Aerosol, 56, 621-671, 10.1029/2018rg000602, 2018.
- 797 Yum, S. S., Hudson, J. G., and Xie, Y.: Comparisons of cloud microphysics with cloud condensation
798 nuclei spectra over the summertime Southern Ocean, 103, 16625-16636, 10.1029/98jd01513,
799 1998.
- 800 Zhang, R., Khalizov, A., Wang, L., Hu, M., and Xu, W.: Nucleation and Growth of Nanoparticles in the
801 Atmosphere, Chemical Reviews, 112, 1957-2011, 10.1021/cr2001756, 2012.

802



803

804 Table 1. A summary of total number concentrations of particles measured with TSI 3776 CPC, TSI

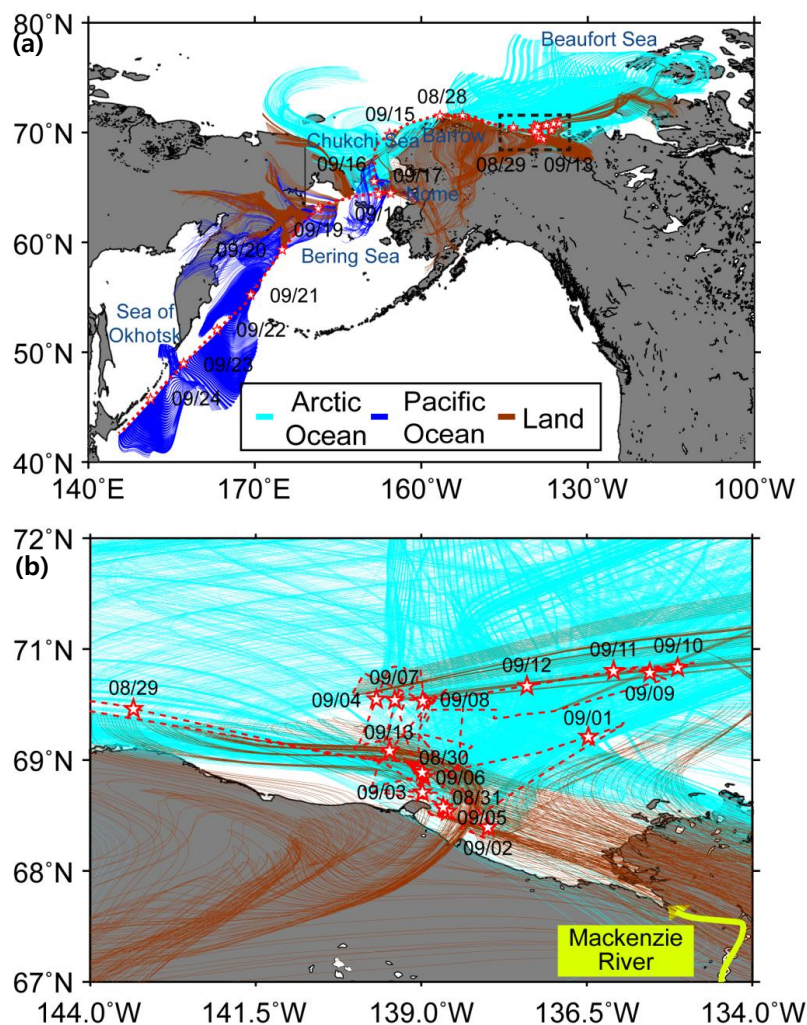
805 3772 CPC, Standard SMPS, and nano SMPS for the three selected periods.

	Pacific Ocean	Arctic Marine	Arctic Terrestrial
Periods	9/21/2017–9/23/2017	9/02/2017–9/05/2017, 9/10/2017–9/12/2017	9/13/2017–9/17/2017
CN _{2.5}	397 ± 185 cm ⁻³	413 ± 442 cm ⁻³	1622 ± 1450 cm ⁻³
CN ₁₀	384 ± 86 cm ⁻³	414 ± 452 cm ⁻³	1396 ± 1279 cm ⁻³
CN _{2.5-10}	35 ± 195 cm ⁻³	62 ± 130 cm ⁻³	263 ± 318 cm ⁻³
N _{Standard SMPS}	224 ± 83 cm ⁻³	204 ± 215 cm ⁻³	739 ± 819 cm ⁻³
N _{nano SMPS}	117 ± 234 cm ⁻³	159 ± 194 cm ⁻³	749 ± 864 cm ⁻³

806

807

808

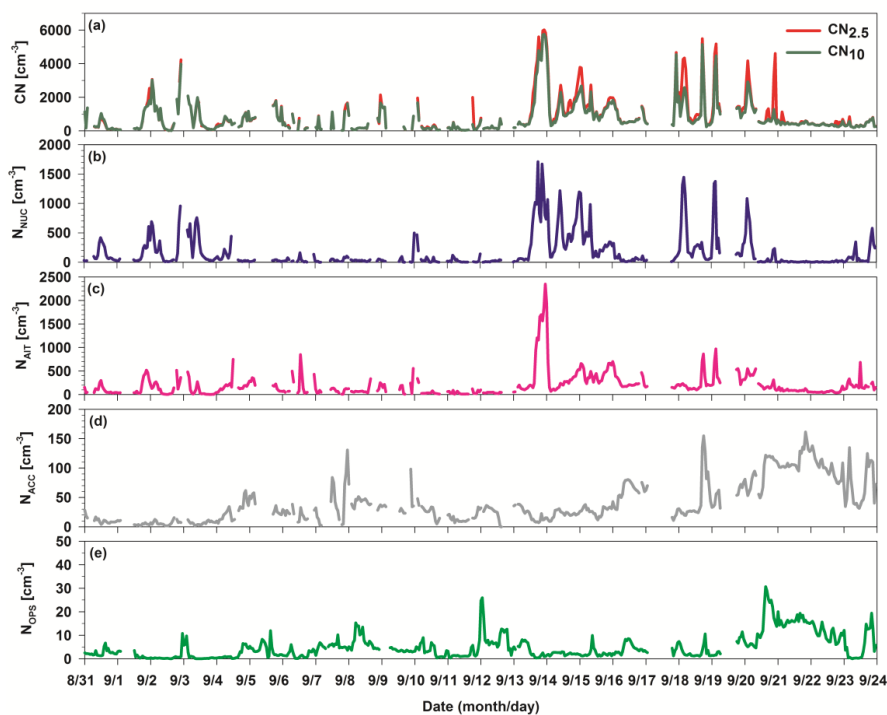


809

810 Figure 1. Ship tracks across (a) the Arctic (8/28/2017–9/18/2017) and Pacific Oceans
811 (9/18/2017–9/25/2017) and (b) zoom into the dotted black square region in Fig. 1a. A dotted red line
812 including star symbols represents ship tracks during the entire cruise. The star symbols represent the
813 daily ship location at midnight. Light blue, blue and brown lines denote the 2-day air mass trajectories
814 categorized into three main domains such as Arctic Ocean, Pacific Ocean, and land, respectively.



815



816

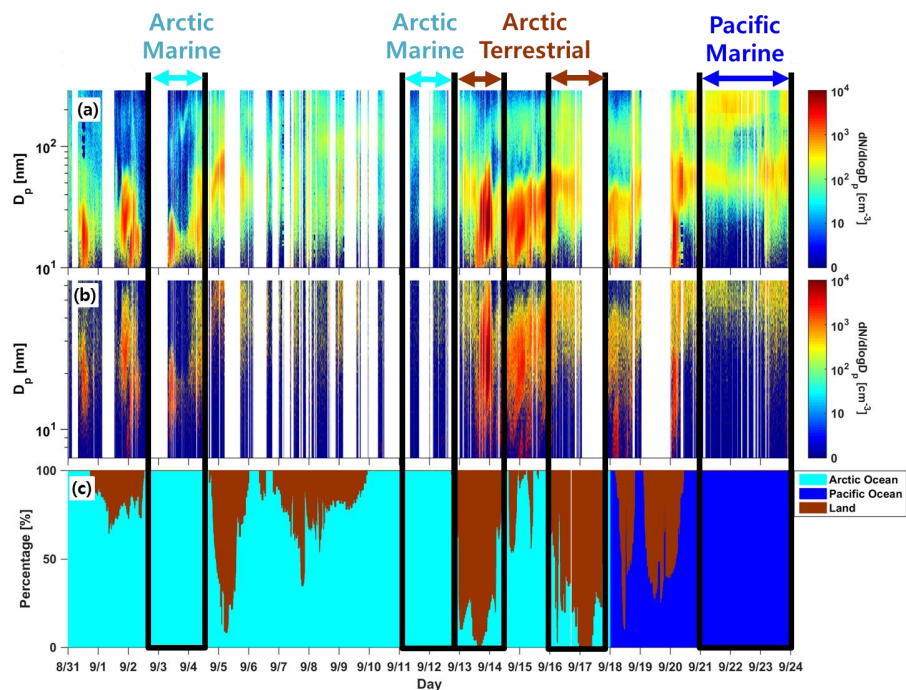
817 Figure 2. Time series of the 1 hour average (a) total aerosol ($CN_{2.5}$ and CN_{10}), (b) nucleation-mode (3 –
818 20 nm) (N_{NUC}), (c) Aitken-mode (20 – 100 nm) (N_{AIT}), (d) accumulation-mode (100 – 300 nm) (N_{ACC}),
819 and (e) coarse-mode (> 300 nm from OPS) (N_{OPS}) number concentrations. The $CN_{2.5}$ and CN_{10}
820 represent total number concentration of particles larger than 2.5 and 10 nm, respectively.

821

822



823

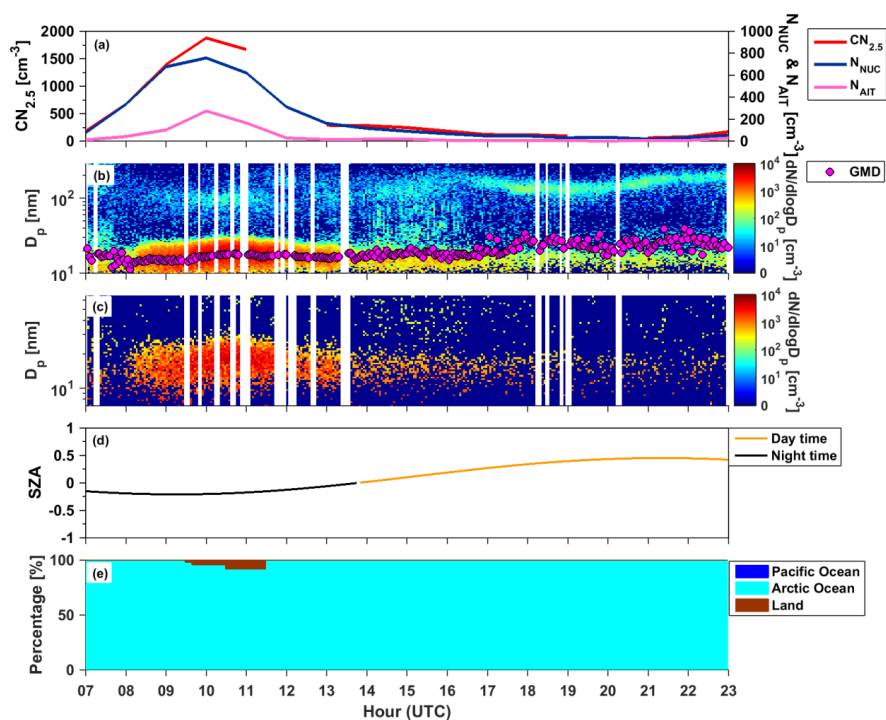


824

825 Figure 3. Contour plots of the size distributions measured using (a) standard and (b) nano SMPS and (c)
826 the residence time of air masses that passed over the Arctic Ocean, Pacific Ocean, and land throughout
827 the sampling periods.



828

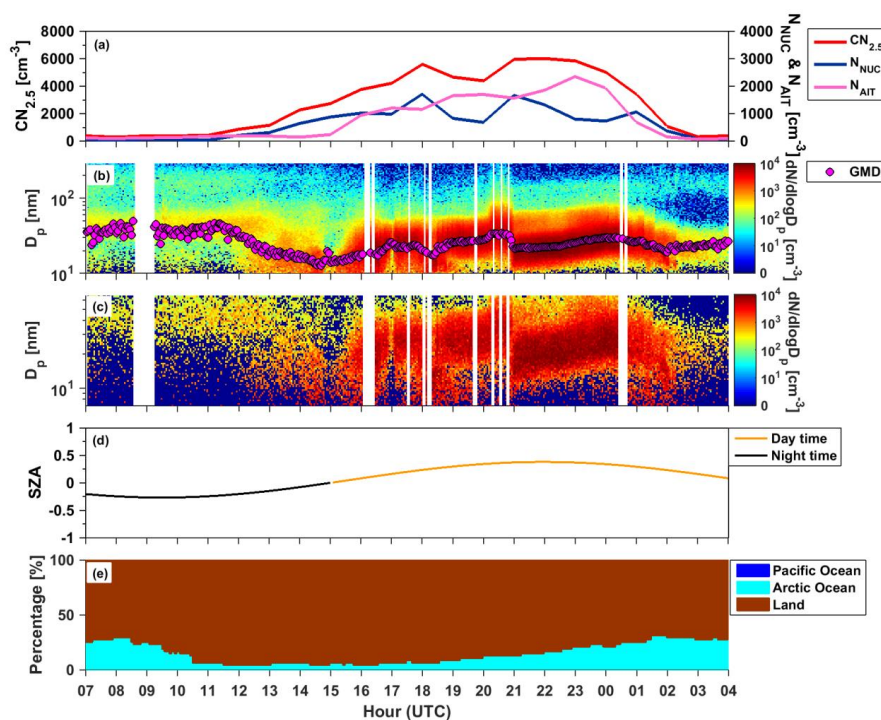


829

830 Figure 4. Example of a case-I event observed on 3 September 2017. From top to bottom, the parameters
831 are: (a) the total number concentration of particles smaller than 2.5 nm, nucleation-mode particles, and
832 Aitken-mode particles; (b) a time series of the standard SMPS size distribution and GMD; (c) a time
833 series of the nano SMPS size; (d) Solar Zenith Angle; (e) the residence time of air masses that passed
834 over the ocean, land, and sea-ice areas.



835

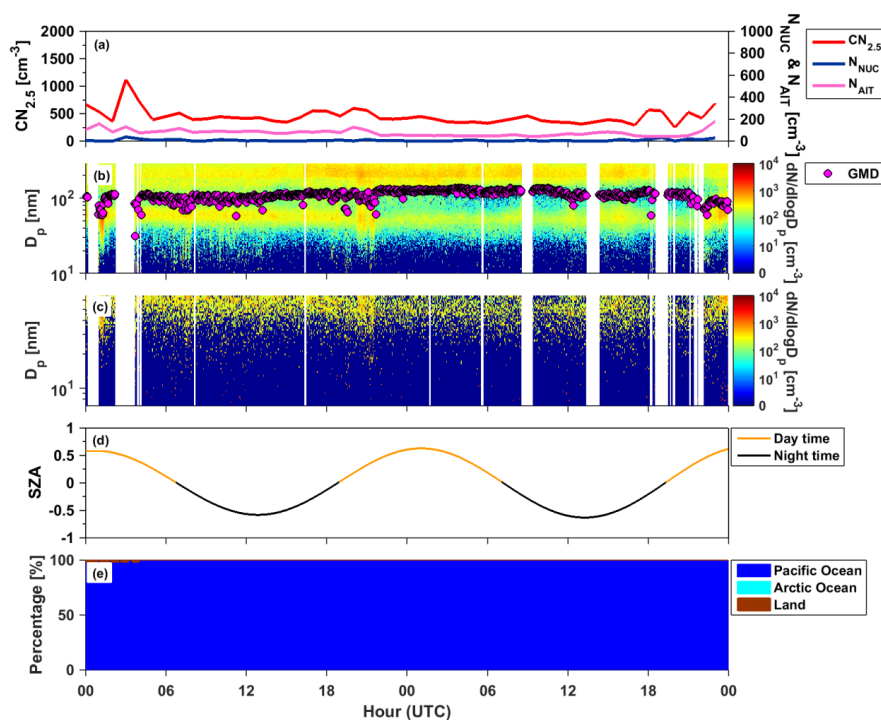


836

837 Figure 5. Example of a case II event that was observed on September 13–14, 2017. From top to bottom,
838 the parameters are: (a) the total number concentration of particles smaller than 2.5 nm, nucleation-mode
839 particles, and Aitken-mode particles; (b) a time series of the standard SMPS size distribution and GMD;
840 (c) a time series of the nano SMPS size; (d) Solar Zenith Angle; (e) the residence time of air masses that
841 passed over the ocean, land, and sea-ice areas.



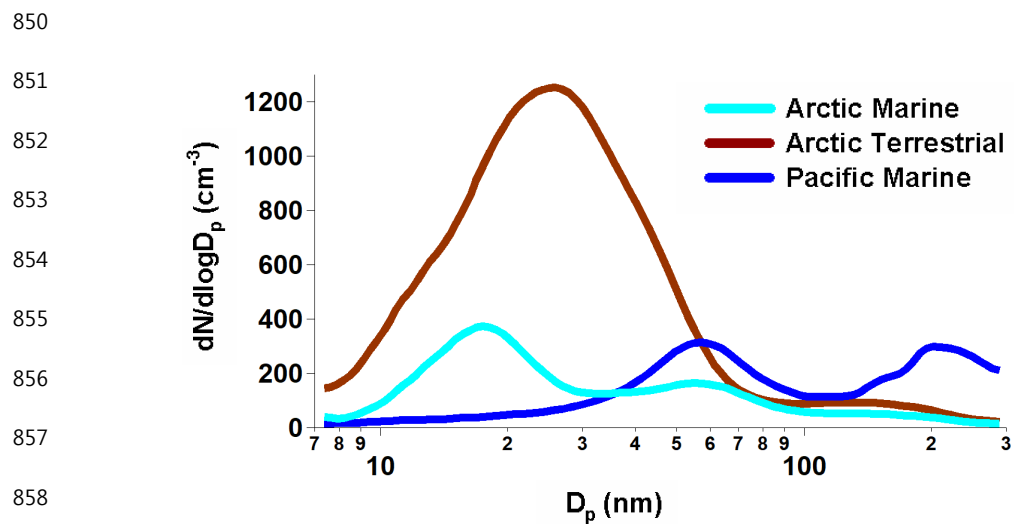
842



843

844 Figure 6. Example of a case III event that was observed on September 21–22 2017. From top to bottom,
845 the parameters are: (a) the total number concentration of particles smaller than 2.5 nm, nucleation-mode
846 particles, and Aitken-mode particles; (b) a time series of the standard SMPS size distribution and GMD;
847 (c) a time series of the nano SMPS size; (d) Solar Zenith Angle; (e) the residence time of air masses that
848 passed over the ocean, land, and sea-ice areas.

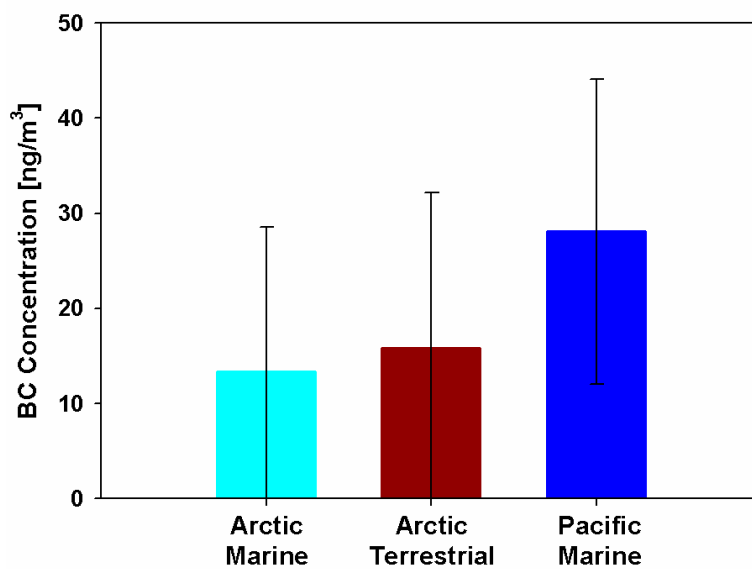
849



859 Figure 7. Average size distributions of aerosol particles for Arctic marine, Arctic terrestrial and Pacific
860 marine air masses
861



862

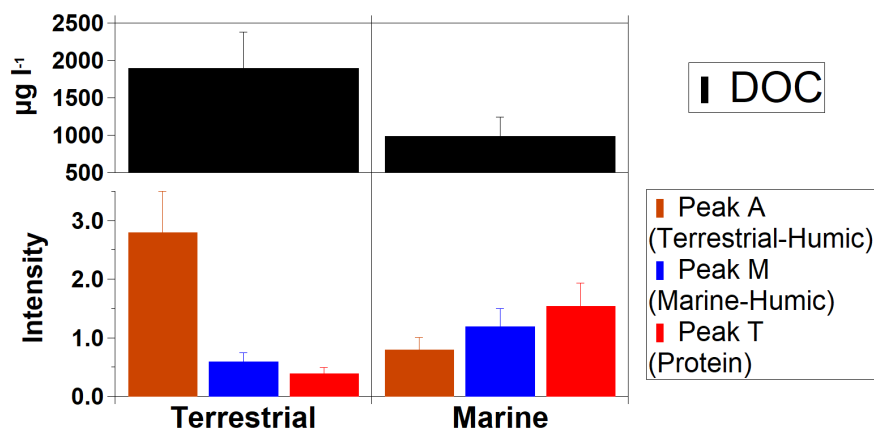


863

864 Figure 8. Average mass concentrations of black carbon for each air mass.



865



866

867 Figure 9. Average DOC concentrations for surface seawater samples collected during this cruise,
868 simultaneously during the atmospheric measurements herein reported. Peak A, M, and T represent
869 terrestrial-humic substances, marine-fulvic substances, and protein, respectively.

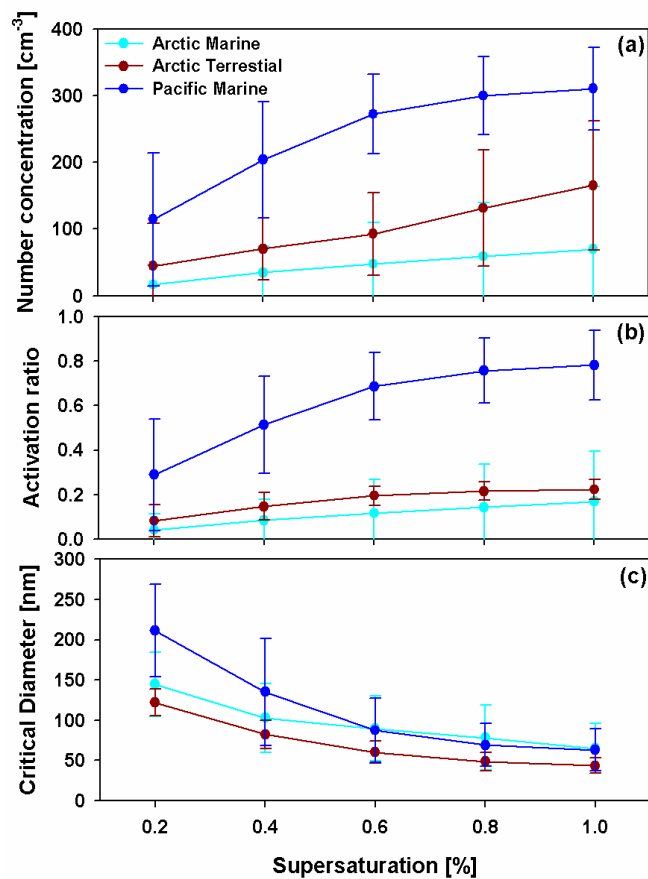
870

871

872



873



874

875 Figure 10. Comparisons of (a) CCN number concentrations, (b) CCN activity, and (c) critical diameter
876 for Arctic marine, Arctic terrestrial and Pacific marine air masses under different supersaturation
877 conditions. The error bars represent a standard deviation.